

Article

Study on the Effect of Vibrating Process on the Compactness of Slipform Concrete

Min Chai ¹, Changbin Hu ^{1,*} and Mingyue Cheng ^{1,2}¹ College of Civil Engineering, Fuzhou University, Fuzhou 350108, China² Jiangxi Tellhow Animation College, Nanchang 220052, China

* Correspondence: huchangbin@fzu.edu.cn

Abstract: Compaction directly affects concrete's strength and durability. In this paper, the relationship between vibration parameters and compactness is modeled by using colored aggregates and image methods to analyze the compactness of concrete characterized by pore structure. Experiments were conducted to investigate the effects of vibrating frequency and duration on the aggregate distribution coefficient, segregation rate, and porosity of slipform concrete. The test results showed that the smaller the aggregate size under high-frequency pounding, the better the concrete compactness. In addition, the aggregate segregation rate and concrete strength increased and then decreased with the pounding length, and the greater the pounding frequency, the more pronounced the trend. Lastly, the concrete's internal porosity increased and then decreased with the pounding length. This study obtained the control range of aggregate segregation rate and porosity through analysis, and established equations for the optimal vibration parameters and paving speed of sliding form concrete to guide the reasonable control of actual sliding form paving and vibration construction processes.

Keywords: vibrating process; sliding form concrete; intensity of the concrete; hole structure



Citation: Chai, M.; Hu, C.; Cheng, M. Study on the Effect of Vibrating Process on the Compactness of Slipform Concrete. *Appl. Sci.* **2023**, *13*, 8421. <https://doi.org/10.3390/app13148421>

Academic Editor: Giuseppe Lacidogna

Received: 27 June 2023

Revised: 16 July 2023

Accepted: 18 July 2023

Published: 21 July 2023



Copyright: © 2023 by the authors. Licensee MDPI, Basel, Switzerland. This article is an open access article distributed under the terms and conditions of the Creative Commons Attribution (CC BY) license (<https://creativecommons.org/licenses/by/4.0/>).

1. Introduction

Cement concrete is widely used in airport road surfaces because of its high strength, high stiffness, good integrity, and high economy [1–3]. As the volume of cement concrete roadway projects increases every year, the inefficiency and cost of manual construction also increase, causing the trend of intelligent roadway construction to become more evident. Roadway slipform concrete construction [4] is becoming an inevitable trend in the future [5]; however, the performance requirements of roadway slipform concrete are more stringent to match [6]. Vibrating is the key link to ensure the performance of concrete [7,8]. However, the actual slipform concrete paving process mainly relies on the pavers to set the vibrating parameters and paving speed according to their experience. The lack of scientific guidance can cause the concrete to be prone to under- or over-vibration. Therefore, improving the quality of slipform concrete paving is important.

Scholars have concluded that freshly mixed concrete has a certain degree of stability under the combined effect of plastic viscosity and yield stress when lightly vibrated or left to stand. With the increase in vibration strength, the plastic viscosity contributes much more to its stability than the yield stress and has a critical role [9]. Scholars have also theoretically analyzed the interrelationship between shear rate and shear stress, and put forward the intrinsic theoretical equations of freshly mixed concrete [10]. Concrete is denser under the high-frequency vibration process, which reduces the defects on the surface of aggregate mortar, and has an improved effect on bending tensile strength and fatigue strength [11]. When the vibrating rod is working, the internal liquefaction region appears near the vibrating rod due to the shear effect, and liquefaction in the peripheral area is mainly due to the action of compressed waves propagating, which is defined as the radius of vibration action [9]. The greater the frequency or acceleration of vibration, the greater

the radius of the corresponding vibration action, and the better the effect of liquefaction on concrete [12–14]. The vibration energy of the concrete in the forward direction of the vibrating rod will increase first and then decrease [15].

Based on the principle of concrete vibration densification, Date et al. observed the densification corresponding to the state of vibration by varying the admixture and sand rate of freshly mixed concrete and found that the vibration densification was higher as the admixture and sand rate increased [16]. Cook proposed the Box-Test method to evaluate the workability of slipform concrete after high-frequency vibration [17]. For slipform concrete, its construction performance has a close relationship with the concrete mix ratio [18–20], but also with the vibration frequency, radius of action, and amplitude of the vibrating rod. This discovery has an important role in guiding the improvement of the smoothness of slipform concrete and the prevention of caving in the actual construction process [21]. Internal air bubbles will directly affect the concrete's compactness. After mixing an appropriate amount of air-entraining agent in slipform concrete, a large number of tiny bubbles can promote vibration liquefaction, reduce the resistance of paving construction, and improve its overall performance [22]. Hansen et al. analyzed the relationship between the frequency of vibration, vibration time, and bubble discharge through the test and concluded that the ideal vibration time of the vibrating rod is 25 s and the vibration spacing should not be greater than 160 mm [23]. The air content inside the concrete will be significantly reduced under high-frequency vibration, and proper vibration can improve the bubble structure of concrete, while over-vibration will lead to a bubble structure with a tendency to deteriorate [24]. Ram found that with the increase in the initial pore content of concrete, the non-homogeneity of the concrete structure increases, and the compressive strength and splitting strength of concrete are reduced [25].

Scholars have studied the relationship between vibration parameters and slipform concrete performance. However, there is a lack of guiding research on engineering field construction. Therefore, this study conducted research on the compactness of slipform concrete under high-frequency vibratory pounding. It also proposed the equation of slipform paving vibration parameters and paved a test section of an airport road surface. The test section of the overall concrete forming effect showed no significant collapse of the edge, slippery shoulder, or falling corner, and the degree of concrete compactness was good. This study of the slipform concrete vibrating construction process can provide theoretical guidance for the large-scale application of slipform paving construction on airport road surfaces.

2. Test

2.1. Raw Material and Matching Ratio

Concrete raw materials were 52.5% road silicate cement (P-I), Minjiang river sand with a fineness modulus of 2.79, colored aggregates, naphthalene as a water-reducing agent, triterpene saponin as an air-entraining agent, and polyacrylamide as a thickening agent. The aggregates were made of naturally colored aggregates, with each grade corresponding to a specific color (Figure 1), to facilitate the study of the effect of vibrating parameters on the internal aggregate distribution of slipform concrete. In this study, 4.75 mm–9.5 mm, 9.5 mm–16 mm, and 16 mm–31.5 mm aggregates corresponded to black, gray, and red, respectively. The physical properties of sand and aggregate are shown in Tables 1 and 2, and the slipform concrete mix ratio is shown in Table 3.

The dosage of water reducing agent, thickener, and air-entraining agent in Table 3 is the percentage of their own dosage and cement dosage.

2.2. Specimen Fabrication and Handling

2.2.1. Specimen Fabrication

This study loaded the freshly mixed slipform concrete into a test mold of 180 mm × 150 mm × 550 mm dimension and inserted the high-frequency pounding bar to vibrate the concrete at a frequency of 6000 r/min, 8000 r/min, and 10,000 r/min

at the pounding durations of 20 s, 30 s, . . . , 110 s. The preparation plan is shown in Table 4 After 24 h, the specimens had hardened and de-molded, and after marking, these were placed in the standard curing room for 28 days. The production process is shown in Figure 2.



Figure 1. Natural colored aggregates of different particle sizes.

Table 1. Physical properties of river sand.

Physical Property	Test Value	Physical Property	Test Value
Apparent density (g/cm^3)	2.65	Ruggedness (%)	2.9
Bulk density (g/cm^3)	1.60	Water absorption rate (%)	0.60
Crushing value (%)	12.77	4.75 mm	Alkali activity test (%)
	12.33	2.36 mm	0.02
	11.73	1.18 mm	Void ratio (%)
	12.07	0.6 mm	41.42
		Chloride ion content	0.0047
		Mud content (%)	0.85

Table 2. Physical properties of colored aggregates.

Types of Colored Aggregates	Particle Size Range (mm)	Apparent Density (kg/m^3)	Bulk Density (kg/m^3)	Water Absorption Rate (%)	Needle-Shaped Particles (%)
Ferrous ore Aggregate	4.75~9.5	2.68	1.51	0.18	1.6
Gray ore aggregate	9.5~16	2.63	1.49	0.34	1.2
Red ore aggregate	16~31.5	2.62	1.49	0.32	2.1

Table 3. Slipform concrete ratio.

Cement	$\rho/\text{kg}\cdot\text{m}^{-3}$			Water-Reducing Agent (%)	Thickening Agent (%)	Air-Entraining Agent (%)
	Aggregate	Sand	Water			
380	1139.8	759.84	144.4	1	0.4	0.5

Table 4. Concrete specimen preparation program.

Serial Number	Vibrating Duration (s)	Vibration Frequency (r/min)	Number of Test Pieces	Serial Number	Vibrating Duration (s)	Vibration Frequency (r/min)	Number of Test Pieces
1	20	6000	3	16	70	6000	3
2		8000	3	17		8000	3
3		10,000	3	18		10,000	3
4	30	6000	3	19		6000	3
5		8000	3	20		8000	3
6		10,000	3	21		10,000	3

Table 4. Cont.

Serial Number	Vibrating Duration (s)	Vibration Frequency (r/min)	Number of Test Pieces	Serial Number	Vibrating Duration (s)	Vibration Frequency (r/min)	Number of Test Pieces
7		6000	3	22		6000	3
8	40	8000	3	23	90	8000	3
9		10,000	3	24		10,000	3
10		6000	3	25		6000	3
11	50	8000	3	26	100	8000	3
12		10,000	3	27		10,000	3
13		6000	3	28		6000	3
14	60	8000	3	29	110	8000	3
15		10,000	3	30		10,000	3



(a) Concrete loading



(b) High-frequency vibratory molding

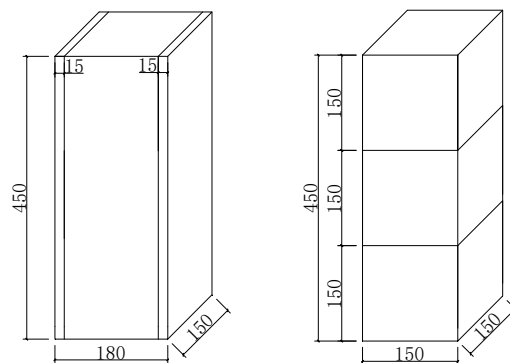


(c) Standard maintenance

Figure 2. Vibratory forming of specimens.

2.2.2. Specimen Cutting

After maintaining for 28 days, the specimens were cut from the bottom to 450 mm, and the column sections were retained. Then, the specimens were cut according to the direction of pounding and forming from both sides to 15 mm inward, respectively. Two clear and distinct sections with an obvious distinction of aggregate color could be obtained from the cutting surface. Finally, the column section was cut into small test pieces into equal parts from top to bottom with a height of 150 mm, and the cutting scheme and results are shown in Figure 3.



(a) Sample cutting plan



(b) Specimen cutting instrument

Figure 3. Cont.

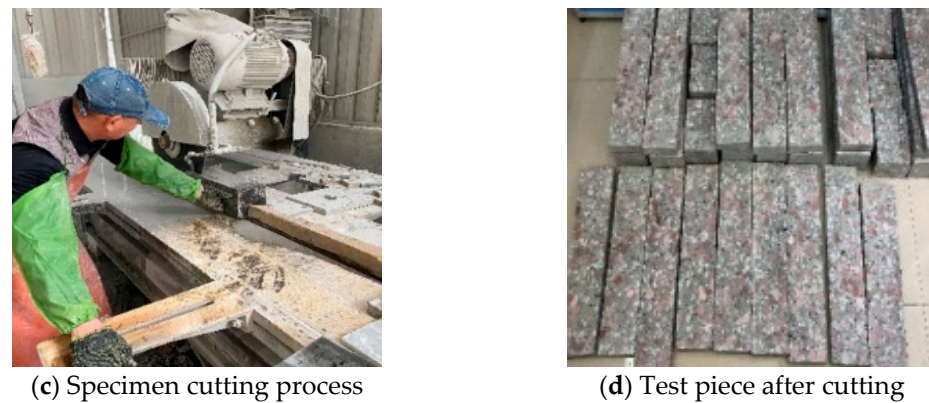


Figure 3. Specimen cutting.

2.2.3. Interface Image Processing

Rectangular specimens (15 mm × 150 mm × 450 mm) cut on both sides of the slipform concrete specimens were ground, polished, and cleaned sequentially. After the moisture on the specimen cross-section evaporated, the cross-sectional images were captured using a digital camera. The images were then processed with Image-Pro Plus image analysis software to accurately separate the different colored aggregates and macroscopic pores from the slurry. This procedure was done to obtain the distribution of all the aggregates, different colored grain sizes, and macroscopic pores (Figure 4).

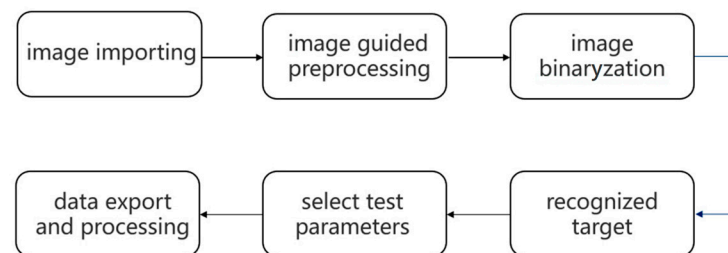


Figure 4. IPP software processing.

The distribution images of the different colored aggregates were divided into three equal parts from bottom to top, and the proportion of the area of the different colored aggregates in each equal part was calculated. This study calculated the distribution of the different aggregate sizes along the vibratory forming direction separately using Equation (1) to obtain the corresponding aggregate distribution coefficient values. The smaller the value, the more uniform the aggregate distribution was.

$$SI = \sqrt{\frac{\sum_{i=1}^3 (P_i - \bar{P}_i)^2}{3}} \quad (1)$$

where P_i is the ratio of the area of aggregate in the i th aliquot to the area of the aliquot, and \bar{P}_i is the average of P_i in the three aliquots.

3. Analysis of Experimental Results

3.1. Effect of Vibrating Parameters on the Compressive Strength of Slipform Concrete

The average compressive strength of the slipform concrete under different vibrating parameters (Figure 5) showed that the law of change increased first and then decreased with the increase in vibration time. In addition, the higher the vibration frequency, the more significant the change, and the shorter the time for the compressive strength to reach the peak. When the vibration frequency was 6000 r/min, the vibration time was 50–90 s, and the compressive strength of slipform concrete was the largest and had the

most stable change. When the vibration frequencies were 8000 r/min and 10,000 r/min, the vibration times were 40–80 s and 40–70 s, respectively. This study analyzed the cause of concrete slipping in the early vibration stage. It was found that the concrete underwent vibration liquefaction, sinking the whole slab in the vibration liquefaction area to discharge the excess air between the particles, making the components more compact and gradually increasing the compressive strength. The greater the frequency of vibration, the better the liquefaction effect of slipform concrete and the faster the gas is discharged. However, as the vibration duration continued to increase, the large-size aggregates sank continuously in the internal vibration liquefaction area of the concrete, and the mortar and small-size aggregates increased in the concrete's upper part. This mechanism resulted in a decrease in the compressive strength of the upper part of slipform concrete.

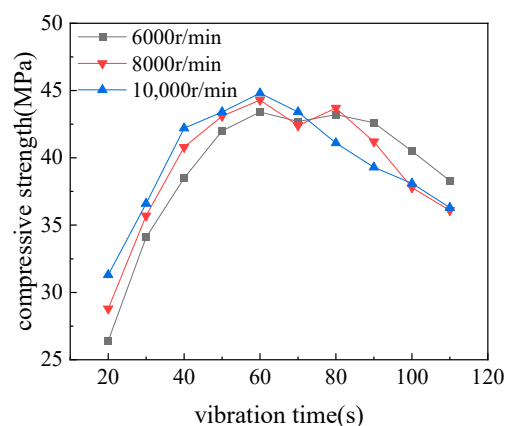


Figure 5. Compressive strength of slipform concrete under different vibrating parameters.

Therefore, the slipform concrete vibrating process should focus on controlling the length of vibrating time to avoid the over-vibration of the concrete.

3.2. Effect of Vibration Parameters on the Distribution of Different Particle Size Aggregates

This study separated the different color aggregates, macroscopic pores, and slurry precisely using Image-Pro Plus software. In addition, it obtained the distribution of all the aggregates, different color particle sizes, and macroscopic pores (Figure 6).

The aggregated size distribution values were calculated for different particle sizes of aggregates at different vibration frequencies of 30 s, 60 s, and 90 s using Equation (1). In addition, the distribution coefficients of different particle sizes of aggregates at different vibration frequencies were plotted (Figure 7).

The results (Figure 7) showed that with the increase in the vibration duration, the distribution coefficient values of different-sized aggregates increased. Therefore, the degree of uniformity of the aggregates became worse. The aggregated distribution coefficient of slipform concrete increased with an increase in vibration frequency for the same pounding duration. In addition, the degree of homogeneity of the different aggregate sizes under the same vibration liquefaction conditions varied significantly. The larger the aggregated size was, the larger and less uniform the aggregated distribution coefficient value became, and the faster the value increased with the increase of the vibration liquefaction effect.

Therefore, when using slipform paving concrete construction, the maximum particle size of the aggregate used should be reduced to maintain the concrete's quality, improve the uniformity of the aggregate in the slipform paving process, and enhance the quality of slipform concrete paving construction.

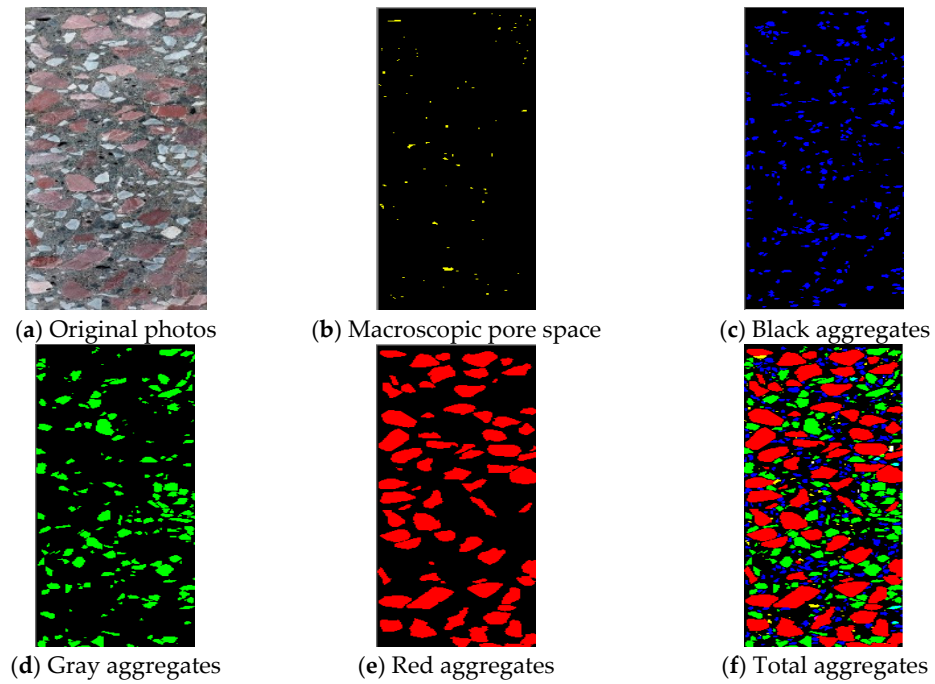


Figure 6. Image analysis of the cut surface of slipform concrete.

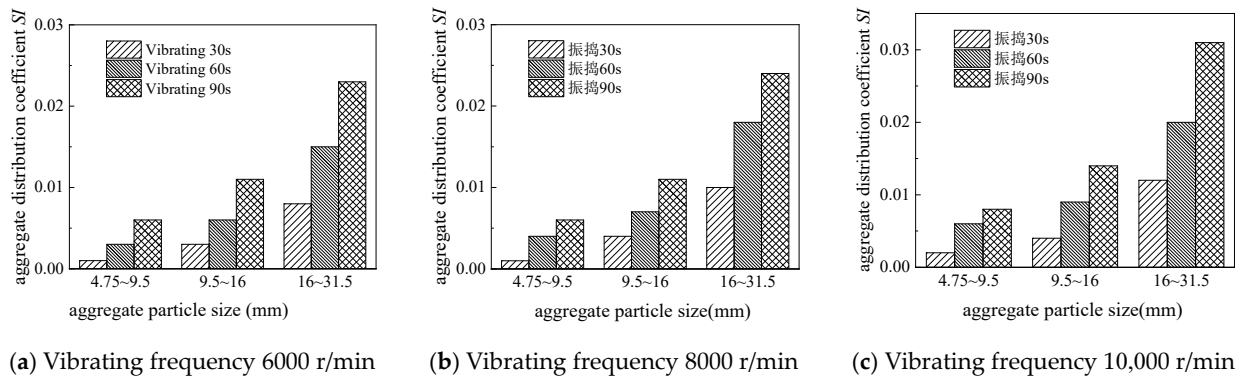


Figure 7. Aggregate size distribution coefficients of concrete under different vibrating parameters.

3.3. Effect of Vibrating Parameters on Segregation of Slipform Concrete

Presently, there is no commonly accepted principle for dissociation testing, and there are few methods for evaluating the dissociation degree. This study defined the SC value as the segregation rate of the degree of bone and paste separation based on the distribution of coarse aggregated area on the cutting surface of slipform concrete specimens (Equation (2)). The smaller the SC value, the lower the degree of homogeneity of aggregate segregation in the vertical direction of the vibratory forming of slipform concrete specimens.

$$SC = \frac{2(P_b - P_t)}{P_b + P_t} \tag{2}$$

where P_t is the area of coarse aggregate within 300–450 mm at the top of the column height, and P_b is the area of coarse aggregate within 0–150 mm at the bottom of the column height.

The SC values of the segregation rate of concrete under the mold with different vibrating parameters were calculated according to Image-Pro Plus image processing (Figure 8).

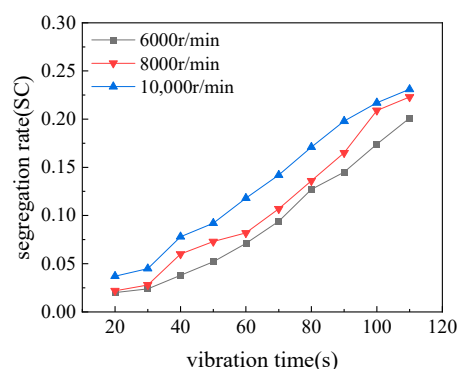


Figure 8. The separation rate of concrete under different vibrating parameters.

The segregation rate's SC value of the slipform concrete increased continuously with increasing vibration time and frequency (Figure 8). These observations showed that the slipform concrete underwent the actions of the high-frequency pounding of the vibration of the vibrating rod near the liquefaction area. These results showed that the large size of the aggregate in the vibration force and self-weight increased its sinking speed. In contrast, the light mass of mortar and some smaller aggregates floated at the top, decreasing the homogeneity of the concrete. Therefore, the proportion of large-size aggregates at the bottom of slipform concrete increased, the mortar and small-size aggregates at the top of concrete increased, and the SC value of the segregation rate increased.

The test results of the compressive strength of slipform concrete under different vibrating parameters showed that the segregation rate SC value influenced the compressive strength of slipform concrete. When the segregation rate SC value was <0.15 , the compressive strength of slipform concrete was affected less. However, when the segregation rate SC value exceeded 0.15, the compressive strength of slipform concrete decreased. Therefore, the SC value <0.15 should be used for the slipform paving with large thicknesses of concrete.

When testing large thicknesses of hardened slipform concrete pavement, the core samples can be analyzed to calculate their segregation rate SC values and determine whether the quality of the concrete is affected by over-vibration.

3.4. Effect of Vibrating Parameters on the Macroscopic Porosity of Slipform Concrete

3.4.1. Effect of Vibrating Duration on the Macroscopic Pore Distribution of Slipform Concrete

Image processing analysis on the cut surfaces of the experimental specimens, using Image-Pro Plus software IPP6.0, obtained the distribution of macroscopic pores on each group of cross-sections. The macroscopic pore distribution of the specimen cross-section was obtained at a vibration frequency of 8000 r/min and vibration time of 20, 40, 50, 60, 90, and 110 s (Figure 9).

With the increase in vibration time, the macroscopic pores inside the concrete gradually decreased (Figure 9). At the early vibration stage, air bubbles of large pore sizes were rapidly discharged from the bottom of the concrete. During the vibrating time period of 20–40 s, the concrete had large pores, mainly distributed in the middle and upper parts of the specimen. When the vibration time was 50–60 s, the large pores were discharged from the concrete. In contrast, only a few small pores were observed inside the concrete when the vibration time was 90–110 s. Therefore, the under-vibration of the actual slipform paving process can be determined by observing the discharge of large air bubbles in the area of the vibration chamber.

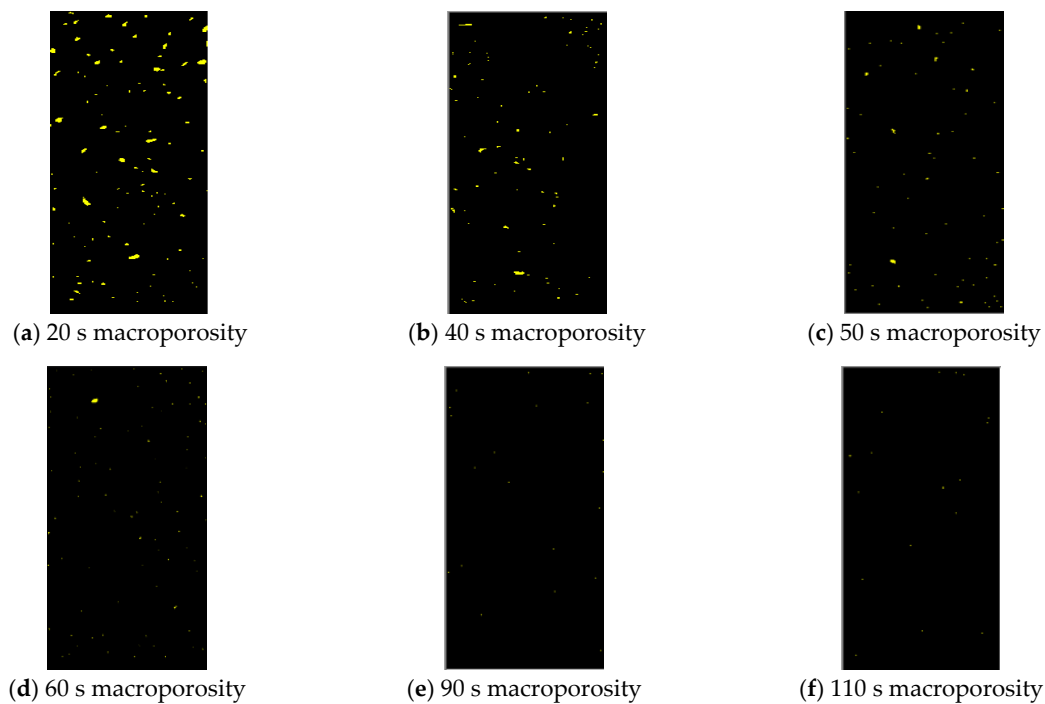


Figure 9. The macroscopic pore distribution of concrete at 8000 r/min pounding frequency.

3.4.2. Effect of Vibration Frequency on the Macroscopic Pore Distribution of Slipform Concrete

The macroscopic pore distributions for the 20, 60, and 90 s of vibration were 6000 r/min and 10,000 r/min, respectively (Figures 10 and 11). Combined with Figure 9, greater vibration frequencies had more significant effects on the discharge of large-diameter air bubbles inside the concrete at the early stage of vibration. In contrast, with the increase in vibration time, the change in small-diameter pores inside was not obvious. It showed that increasing the vibration liquefaction effect of slipform concrete by increasing the vibration frequency impacted the rapid discharge of large-diameter air bubbles positively inside the concrete. In contrast, the effect on small-diameter air bubbles was relatively small.

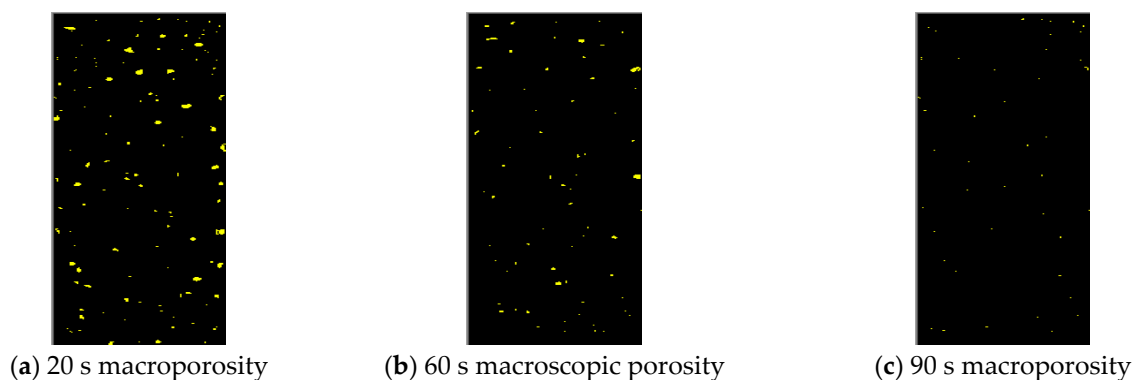


Figure 10. Vibration frequency of 6000 r/min under the macroscopic pore distribution of concrete.

3.4.3. Effect of Vibration Parameters on Macroscopic Porosity

Macroscopic porosity is the macro porosity area-to-section area ratio, P . When P was higher, the macro porosity was greater, and the denseness degree was smaller. The study calculated the average value of the macroscopic porosity of the specimen under different vibrating parameters (Figure 12).

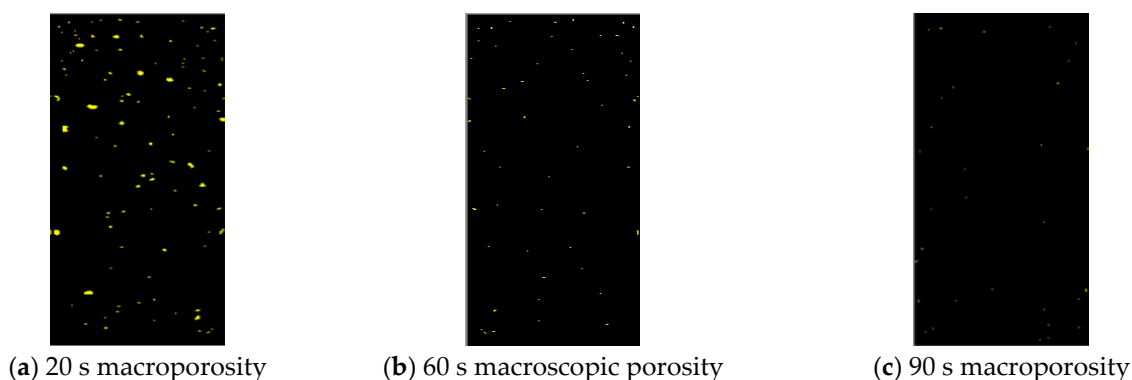


Figure 11. Vibration frequency of 10,000 r/min under the macroscopic pore distribution of concrete.

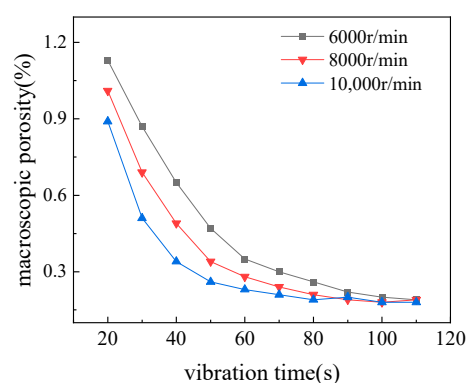


Figure 12. Macroscopic porosity of concrete under slip molds with different vibrating parameters.

In the early stages of slipform concrete vibration, the p decreased rapidly with a higher frequency of vibration. With the increase in vibration time, p was $<0.3\%$, and the change in macroscopic porosity gradually leveled off, consistent with the macroporosity distribution change law. At the early stage of vibration, large-diameter air bubbles discharged rapidly, the macroscopic pore area inside the concrete decreased substantially, and p decreased rapidly. With the increase in vibration time, the large bubbles became exhausted, and the concrete internals had small bubbles due to their slow uplift. Therefore, the late vibration macroporosity p value changes gradually weakened.

A comprehensive comparison of different vibrating parameters under the compressive strength of slipform concrete showed that the macroporosity scores $<0.3\%$ were in line with the requirements. In addition, less basic concrete specimens on the cross-section of macroporosity had no large-diameter pores. Therefore, the proposed macroscopic porosity $p < 0.3\%$ was qualified. When the vibration frequency is 6000 r/min, 8000 r/min, and 10,000 r/min, the vibration time should not be <70 , <60 s, and <50 s, respectively.

4. Optimal Vibrating Parameter Equation and Paving Speed Equation

4.1. Equation of Optimal Vibrating Parameters

This study determined the optimum vibrating time T at different vibrating frequencies according to the compressive strength, segregation rate SC value, and macroscopic porosity p value of slipform concrete (Table 5).

For airport road surface slipform concrete, the strength and the macroporosity requirements of a large thickness (≥ 42 cm) should be met. The comprehensive analysis showed that when the vibrating frequencies were 6000 r/min, 8000 r/min, and 10,000 r/min, the best vibrating time were 70–90 s, 60–80 s, and 50–70 s, respectively (Table 2). The ball test measured the time t of the ball rising at different vibration frequencies and vibration coefficient K value (Table 6).

Table 5. Optimal vibrating time for concrete with different pounding frequencies under the mold.

Performance Requirements	Optimum Vibrating Time (s)		
	6000 r/min	8000 r/min	10,000 r/min
Compressive strength	$50 \leq t \leq 90$	$40 \leq t \leq 80$	$40 \leq t \leq 70$
Macroporosity	$70 \leq t$	$60 \leq t$	$50 \leq t$

Table 6. Ranges of vibrating coefficient K values for different vibrating parameters.

Vibrating Frequency	T	t	$K = t_1/t$
6000 r/min	70~90 s	45.7	$1.53 \leq K \leq 1.97$
8000 r/min	60~80 s	31.7	$1.61 \leq K \leq 2.14$
10,000 r/min	50~70 s	30.2	$1.66 \leq K \leq 2.32$

The comprehensive analysis of the compressive strength of slipform concrete, segregation rate SC , and macroporosity p value, the optimum range of the vibration coefficient K value was determined to be 1.60~2.00.

The time T and height h of the ball rising in the small ball test had a mathematical relationship with the vibration viscosity coefficient η . Therefore, the public t was substituted with the vibration viscosity coefficient η , and the equation of the vibrating time length T and the vibration viscosity coefficient η were further deduced (Equation (3)).

$$T = K \frac{H\eta}{78.2747(\rho_C - 0.0858)}, \tag{3}$$

where ρ_C is the volumetric weight of concrete (g/cm^3), H is the rise height of the small ball ≥ 42 cm, η is the vibration viscosity factor (Ns/m^2) at 10 cm from the pounding bar, and T is the required vibration time of concrete (s) at the corresponding vibration frequency.

4.2. Paving Speed Equation

This study laid out its vibrating bar based on the GOMACO GP-2400 slipform paver (Figure 13a). When the paver was working, the vibrating bar was rotated from horizontal to downward at an angle of θ to obtain a better-vibrating effect (Figure 13b). The actual length of the vibrating bar was L . Assuming that the propagation direction of the vibration wave impact generated at any point of the vibrating bar is perpendicular to the vibrating bar, the length of the vibrating effect of the vibrating bar at any point in the corresponding vibrating area after the θ , angle rotation of the vibrating bar downward is $L/\cos\theta$. The paving speed V of the slipform paver was deduced from Equation (3) (Equation (4)).

$$V = \frac{60L}{Kt \cdot \cos\theta} \tag{4}$$

where L is the length of the Concrete vibrating rod (m), θ is the angle between the pounding bar and the horizontal direction, and V is the vibrator frequency corresponding to the small ball experiment sliding die paving speed (m/min).

The equation for the paver travel speed V and the vibration viscosity coefficient η were derived (Equation (5)) by substituting t in Equation (3) with the vibration viscosity coefficient η .

$$V = \frac{4696.482L(\rho_C - 0.0858)}{KH\eta \cdot \cos\theta} \tag{5}$$

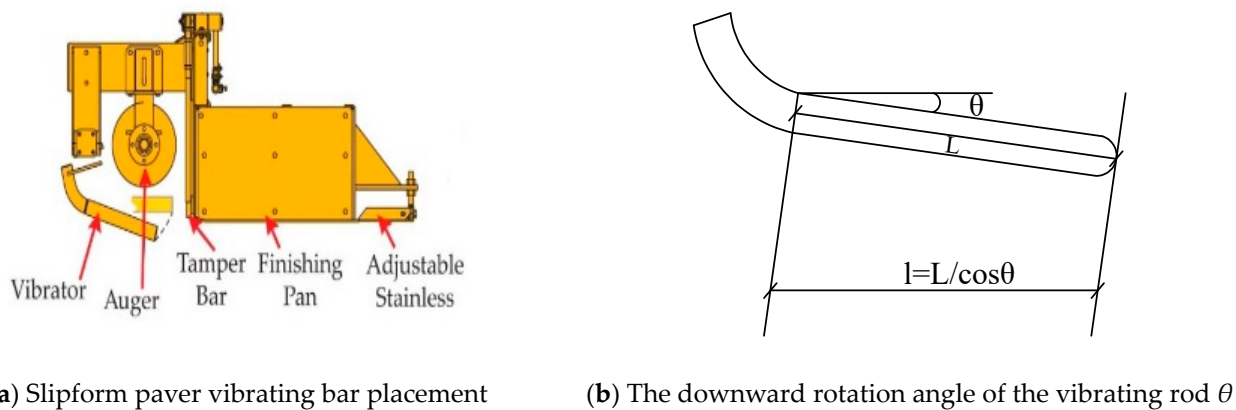


Figure 13. GP-2400 Slipform paver vibrating bar placement and deflection angle.

5. Engineering Applications

Relying on Chengdu Tianfu International Airport, a slipform paving test was conducted using a GOMACO GP-2400 slipform paver with a concrete pavement length, width, and height of 25 m, 5 m, and 0.42 m, respectively. The raw materials and the concrete mix ratio used in the test section were the same as those used in the indoor test (Table 1).

Before paving, the vibrating rod, the horizontal angle θ , and the vibrating frequency of the rod were set to 15 and 8000 r/min, respectively. The indoor test measured that the vibrating frequency of 8000 r/min for 33.7 s rose 42 cm under the mold concrete sphere. The vibrating frequency of the outermost vibrating rod on both sides is adjusted to 1000 r/min in a field test section of slipform paving construction to ensure that both sides of the Yin and Yang Enterprise mouths were densely formed (Figure 14).

This study observed a high vibrating performance of slipform concrete and a fast speed of slurry, which met the requirements of site construction (Figure 14). In addition, there was a high overall forming effect of the road surface and no large collapsed edges in the concrete, slippery shoulders, or fallen corners. Therefore, the Yin and Yang Enterprise mouths were more completely retained and vibrated compactly.



(a) On-site fabric



(b) Vibratory liquefaction of concrete



(c) The effect of the surface layer after smoothing with the smoother



(d) The effect of the surface layer after manual smearing

Figure 14. Cont.



(e) The effect of shaping the test section's Yang Enterprise mouth (f) The effect of shaping the shaded mouth of the test section

Figure 14. Slipform paving test at Chengdu Tianfu International Airport.

This study took cores from the road surface after 28 days of curing (Figure 15) to examine the macroscopic pores on the surface. It was observed that the large pores were discharged, the overall concrete was well compacted, and the separation rate SC was <0.15 .



Figure 15. Core samples from the test section coring.

The overall effect of the actual slipform paving and vibrating construction of the test section was roughly the same as the indoor experimental results. After vibrating and forming, there is no collapse of edges, shoulders, and corners, and the fresh concrete has high cohesiveness and complete and dense retention of Yin and Yang openings. In addition, the equations for the optimum vibration parameters and paving speed for slipform construction were feasible and showed significant reasonable control of the field vibration construction process of slipform paving of large-thickness concrete.

6. Discussion

Based on the above experiments and a comparison of existing domestic and foreign research results, it can be seen that:

(1) Through research, it was found that under high-frequency vibration, the larger the particle size of coarse aggregate, the worse its uniformity. This result is consistent with the current research findings. Wu Bin of the Wuhan University of Technology also found that the gradation of coarse aggregate has a greater impact on the stability of concrete. The greater the content of large-size aggregate, the worse the stability of concrete and the more prone to segregation [9]. So, while ensuring the quality of sliding form concrete, the maximum particle size of coarse aggregate should be reduced to improve the stability and homogeneity of concrete during paving and vibrating construction.

(2) This article studies the relationship between compressive strength and segregation rate SC value during aggregate vibration segregation. It is found that the compressive strength of concrete begins to decrease when the segregation rate SC value is greater than 0.15.

At present, there is no unified standard for the evaluation method of concrete segregation, and the most commonly used method is the segregation degree SD [26]. This method is mainly based on the digital image processing method and the assumption that the coarse aggregate is evenly distributed in the volume space, and characterizes the segregation

degree of the aggregate inside the concrete by establishing a radial continuous distribution model of the coarse aggregate. Table 7 shows the Comparative analysis of SD and SC.

Table 7. Comparative analysis of SD and SC.

Serial Number	SD [26]. (Segregation Degree)	SC (Segregation Rate)
1	0.017	0.04
2	0.031	0.04
3	0.040	0.10
4	0.045	0.13
5	0.047	0.15
6	0.050	0.10
7	0.061	0.20
8	0.089	0.12
9	0.088	0.14
10	0.100	0.16
11	0.109	0.16
12	0.120	0.34

Yancong proposed in the experiment that *SD* greater than 0.10 is severe segregation, and the quality of concrete begins to be significantly affected [26]. From the table, it can be seen that when the *SD* value is less than 0.1, according to the evaluation method for coarse aggregate segregation in this article, the segregation rate *SC* value of concrete is basically below 0.15. When the *SD* value is greater than 0.10, the *SC* value is greater than 0.15. Through the above comparison, it can be found that there is a certain correlation between the *SC* value of the segregation rate in this article and the *SD* value of the segregation degree proposed by Zhang Yancong, both of which can evaluate the segregation situation of concrete.

In addition, this also indicates that the proposed separation rate of 0.15 as the qualified line in this article has certain feasibility. By removing the influence of data errors, using the segregation rate *SC* value in this article can more conveniently evaluate the segregation of concrete and determine whether the quality of concrete is affected by excessive vibration.

(3) In this paper, an optimal range of vibration coefficient *K* is determined by the mutual restriction of the rising time *t* of the ball in the vibration viscosity coefficient of concrete, the compressive strength, the macroporosity, and the segregation rate, and then the optimal vibration Parametric equation and the paving speed equation are derived based on the construction principle of slip form paving and vibrating.

The method proposed in this article is significantly different from the current research on the vibration time and paving speed of sliding from concrete by researchers. Yuan Yezhen of the Hebei University of Technology and He Lu of the Highway Research Institute of the Ministry of Transport put forward the best vibrating time and paving speed mainly through the relationship between the effective range of action of the vibrating rod and the vibration acceleration [15,27]. This method has significant drawbacks, as it does not take into account the differences in vibration parameters and paving speed corresponding to different states of concrete, and does not consider the impact of vibration frequency, making it not universal.

The vibration parameter equation and paving speed equation proposed in this paper solve these drawbacks, in which the rise time of the ball *t* and the vibration viscosity coefficient can directly characterize the effect of vibration liquefaction of concrete in different states. In the process of actual paving and vibration construction, according to the measured ball rise time *t* or vibration viscosity coefficient of the concrete in the field, the specific vibration parameter and paving speed range corresponding to the concrete can be calculated by substituting into the equations, which has better rationality and practicality.

7. Conclusions

(1) Under the effect of high-frequency vibrating, larger aggregate particle size caused a larger aggregate distribution coefficient value and a lower degree of uniformity. In addition, the value increased at a faster rate under the vibration liquefaction effect. The maximum size of the aggregate used should be reduced to improve the uniformity of the aggregate in the process of slipform paving and enhance the quality of slipform concrete paving and vibrating construction.

(2) The vibrating parameters of the high-frequency concrete vibrating rod significantly influenced the compressive strength and SC value of the aggregate segregation rate of slipform concrete. Compressive strength increased and then decreased with the vibration time. In addition, the higher the frequency of vibration, the faster the rate of change. The rate of aggregate segregation increased with the vibration time, and the higher the frequency of vibration, the more it increased. The SC value of the segregation rate should be <0.15 to avoid adverse effects on the quality of concrete.

(3) The effects of different vibrating parameters on different pore-size bubbles of slipform concrete were different. Large pore-size bubbles were predominantly discharged, the pore area inside the concrete was significantly reduced, and the macroscopic porosity p value was rapidly reduced at the early stage of vibration. With the increase in vibration time, the large bubbles became exhausted, and the small pore-size bubbles were predominantly discharged. However, the tiny bubbles rose to the surface slowly, and the macroporosity p value changes in the late vibration period were slight. Analysis showed that the macroporosity should be $<0.3\%$.

(4) According to the influence of the vibrating parameters on the performance of slipform concrete, the equations for the optimal vibrating parameters and paving speed of slipform concrete were derived by combining the actual paving construction requirements. When slipform paving large thickness (≥ 42 cm) concrete, the range of the optimal vibration coefficient K value was 1.6–2.0, and the optimal vibration parameter equation is:

$$T = \begin{cases} Kt \\ K \frac{H\eta}{4696.482(\rho_C - 0.0858)} \end{cases}$$

The paving speed equation is given by:

$$V = \begin{cases} \frac{60L}{Kt \cdot \cos \theta} \\ \frac{4696.482L(\rho_C - 0.0858)}{KH\eta \cdot \cos \theta} \end{cases}$$

(5) The airport road surface slipform paving field test showed that the engineering practice paving effect and indoor tests were similar. The slipform concrete vibration construction performance and the paving forming overall effect were good, indicating that slipform concrete ratio parameters and admixtures are significant. The overall compactness of concrete after hardening was high, and the SC value of the segregation rate was <0.15 , indicating that the equations of the best vibration parameters and paving speed of slipform construction were feasible. These factors can significantly control the construction process of paving large-thickness concrete in slipform.

Author Contributions: Conceptualization, C.H. and M.C. (Min Chai); methodology, C.H.; software, M.C. (Mingyue Cheng); investigation, M.C. (Mingyue Cheng); resources, C.H.; data curation, M.C. (Min Chai) and M.C. (Mingyue Cheng); writing—original draft preparation, M.C. (Mingyue Cheng); writing—review and editing, M.C. (Min Chai); supervision, C.H.; project administration, C.H.; funding acquisition, C.H. All authors have read and agreed to the published version of the manuscript.

Funding: This research is financially supported by the National Natural Science Foundation of China (Grant No. 51978172).

Institutional Review Board Statement: Not applicable.

Informed Consent Statement: Informed consent was obtained from all subjects involved in the study.

Data Availability Statement: Not applicable.

Acknowledgments: The authors gratefully acknowledge the financial support provided by the Scientific Research Fund of the National Natural Science Foundation of China (51978172).

Conflicts of Interest: The authors declare no conflict of interest.

References

1. Lu, H.; Zhao, C.; Yuan, J.; Yin, W.; Wang, Y.; Xiao, R. Study on the Properties and Benefits of a Composite Separator Layer in Airport Cement Concrete Pavement. *Buildings* **2022**, *12*, 2190. [[CrossRef](#)]
2. Su, J.; Zhou, Z.; Kong, F.; Lai, Y.; Zhang, W. Research and Analysis of Civil Airport Cement Concrete Pavement Damage Condition Evaluation and Countermeasure. *IOP Conf. Ser. Earth Environ. Sci.* **2020**, *510*, 52072. [[CrossRef](#)]
3. Zhang, R.; Qi, C.; Zhang, X. Research on structural damage on cement concrete pavement in the airport. In *ICTIS 2011: Multimodal Approach to Sustained Transportation System Development-Information, Technology, Implementation*; ASCE: Reston, VA, USA, 2011; pp. 2135–2140. [[CrossRef](#)]
4. Wang, K.; Pekmezci, B.Y.; Voigt, T.; Shah, S.P. Low compaction energy concrete for improved slipform casting of concrete pavements. *Aci Mater. J.* **2007**, *104*, 251–258. [[CrossRef](#)]
5. Castro-Lacouture, D. Construction Automation and Smart Buildings. In *Springer Handbook of Automation*; Springer: Cham, Switzerland, 2023; pp. 1035–1053. [[CrossRef](#)]
6. Wang, X.; Taylor, P.; Wang, X. A novel test to determine the workability of slipform concrete mixtures. *Mag. Concr. Res.* **2017**, *69*, 292–305. [[CrossRef](#)]
7. Basler, F.; Auml, M.; Hner, D.; Fischer, O.; Hilbig, H. Influence of early-age vibration on concrete strength. *Struct. Concr.* **2023**, *1*. [[CrossRef](#)]
8. Yan, W.; Cui, W.; Qi, L. DEM study on the response of fresh concrete under vibration. *Granul. Matter* **2022**, *24*, 37. [[CrossRef](#)]
9. Li, Z.; Cao, G. Rheological behaviors and model of fresh concrete in vibrated state. *Cem. Concr. Res.* **2019**, *120*, 217–226. [[CrossRef](#)]
10. Kolawole, J.T.; Boshoff, W.P.; Babafemi, A.J.; Combrinck, R. Shear and viscoelastic properties of early-age concrete using small-amplitude and low-rate rheometry—From fresh state to initial set. *Cem. Concr. Compos.* **2021**, *124*, 104223. [[CrossRef](#)]
11. Banfill, P.F.G.; Teixeira, M.A.O.M.; Craik, R.J.M. Rheology and vibration of fresh concrete: Predicting the radius of action of poker vibrators from wave propagation. *Cem. Concr. Res.* **2011**, *41*, 932–941. [[CrossRef](#)]
12. Li, J.; Tian, Z.; Sun, X.; Ma, Y.; Liu, H.; Lu, H. Modeling vibration energy transfer of fresh concrete and energy distribution visualization system. *Constr. Build. Mater.* **2022**, *354*, 129210. [[CrossRef](#)]
13. Li, L.; Wu, J.; Zhang, Y.; Li, K.; Liu, Y.; Liu, L.; Chen, Y. Research Progress of concrete Vibratory Technology. *Acad. J. Sci. Technol.* **2022**, *3*, 71–77. [[CrossRef](#)]
14. Cai, Y.; Liu, Q.; Yu, L.; Meng, Z.; Hu, Z.; Yuan, Q.; Aavija, B. An experimental and numerical investigation of coarse aggregate settlement in fresh concrete under vibration. *Cem. Concr. Compos.* **2021**, *122*, 104153. [[CrossRef](#)]
15. Date, S.; Goryozono, Y.; Hashimoto, S. Study on Consolidation of Concrete with Vibration. *Phys. Procedia* **2012**, *25*, 325–332. [[CrossRef](#)]
16. Cook, M.D.D.O.; Tyler Ley, M.; Ghaeezadah, A. A workability test for slip formed concrete pavements. *Constr. Build. Mater.* **2014**, *68*, 376–383. [[CrossRef](#)]
17. Cook, M.D.M.C.; Ghaeezadah, A.G.A.G.; Ley, M.T.T.L. Impacts of Coarse-Aggregate Gradation on the Workability of Slip-Formed Concrete. *J. Mater. Civ. Eng.* **2018**, *30*, 04017265. [[CrossRef](#)]
18. Chung, H.; Subgranon, T.; Tia, M. Reducing cementitious paste volume of slipformed pavement concrete by blending aggregates. *Int. J. Pavement Res. Technol.* **2020**, *16*, 679–685. [[CrossRef](#)]
19. Siamardi, K.; Shabani, S.; Mansourian, A. Optimization of concrete mixes using mixture approach for slip-formed concrete pavement incorporating blends of limestone aggregates. *Constr. Build. Mater.* **2023**, *397*, 132377. [[CrossRef](#)]
20. Nassima, K.; Fattoum, K. Stability of Extruded Concrete for Road Safety Barriers and Effect of Mineral Admixtures on Concrete Behaviour. *J. Road Saf.* **2022**, *33*, 45–55. [[CrossRef](#)]
21. Zhang, Y.; Gao, L.; Shen, J. Vibration characteristics of air-entrained concrete based on slipform construction. *Appl. Mech. Mater.* **2012**, *204–208*, 1549–1552. [[CrossRef](#)]
22. Hou, Z.Y.; Yuan, Y.Z.; Yuan, Z.G.; Liang, Y.D.; Zhou, Z.H. Study on Vibrational Liquefaction Behavior of Air-Entrained Concrete. *Adv. Mater. Res.* **2013**, *857*, 20–26. [[CrossRef](#)]
23. Yang, Q.; Zhu, B.; Yang, Q.; Wang, B.; Shu, J. Effects of high-frequency vibration on air void parameters of air-entrained concrete. *J. Build. Mater.* **2007**, *10*, 331–336. [[CrossRef](#)]
24. Zhang, Y.C.; Gao, L.L. Effect of High Frequency Vibration on Pore Parameters and Frost Resistance of Air Entrained Concrete. *Adv. Mater. Res.* **2013**, *671–674*, 1680–1683. [[CrossRef](#)]
25. Ram, P.V.; Van Dam, T.J.; Sutter, L.L.; Anzalone, G.; Smith, K.D. Field Study of Air Content Stability in the Slipform Paving Process. *Transp. Res. Rec. J. Transp. Res. Board* **2014**, *2408*, 55–65. [[CrossRef](#)]

26. Zhang, Y.C.; Gao, L.L.; Wang, D.P. Evaluation Method of Segregation of Road Concrete. *J. Highw. Transp. Res. Dev.* **2012**, *29*, 23–27. [[CrossRef](#)]
27. Yuan, Y.Z.; Tian, B.; Liu, Y.; Hou, Z.Y. Performance study on the slip-form construction feature of air-entrained cement concrete. *Concrete* **2013**, *5*, 147–150. [[CrossRef](#)]

Disclaimer/Publisher’s Note: The statements, opinions and data contained in all publications are solely those of the individual author(s) and contributor(s) and not of MDPI and/or the editor(s). MDPI and/or the editor(s) disclaim responsibility for any injury to people or property resulting from any ideas, methods, instructions or products referred to in the content.